Selectivity and Mechanism of Hydrogen Atom Transfer by an Isolable Imidoiron(III) Complex

Ryan E. Cowley, Nathan A. Eckert, Sridhar Vaddadi, Travis M. Figg, Thomas R. Cundari,* Patrick L. Holland*

1. Introduction

1-1. Hydrogen atom transfer (HAT)

• HAT is an elementary chemical transformation that is utilized in many enzymatic systems such as oxidation by cytochrome P450, methane monooxygenase, ribonucleotide reductases, and so on.[1]

$$A\bullet \quad + \quad H-B \quad \longrightarrow \quad A-H \quad + \quad \bullet B \qquad (1)$$

1-2. Metal–oxo copmplexes

• Extensive studies on HAT reactivity of M=O using *isolated* biomimetic M=O complexes (especially Fe=O).

• Linear correlation between rates of HAT and homolytic bond dissociation energy (BDE) of a C–H bond being broken (faster HAT with smaller BDE) is found regardless of the size of substrates in many cases.[1,2]

$$[M]{=}O^{n+} \quad + \quad H-R \quad \longrightarrow \quad [M]{-}O{-}H^{(n-1)+} \quad + \quad \bullet R \qquad (2)$$

1-3. Metal–imido complexes

• Imido (NR^{2-}) ligands are isoelectronic to oxo (O^{2-}) ligands.

• More versatile than oxo complexes because steric and electronic properties can be tuned by N substituents.

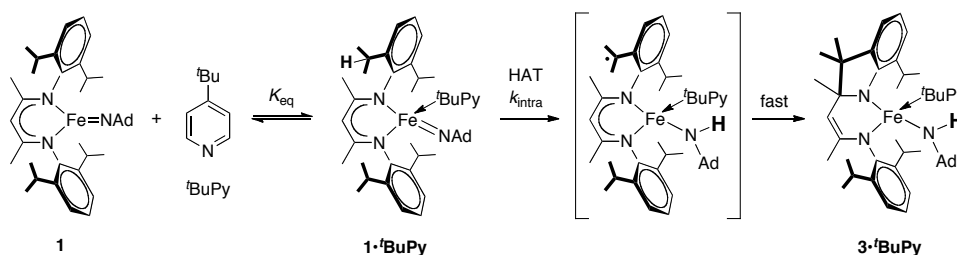• Only a few of *isolated* M=NR complexes that perform HAT reactions.

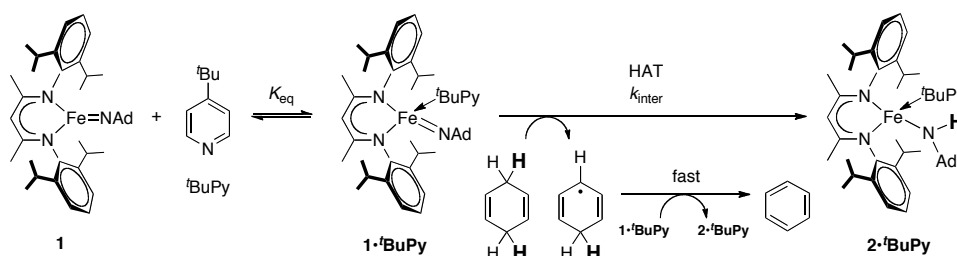➔ HAT reactivity of M=NR has not been well investigated in detail compared to M=O.

$$[M]{=}N{-}R'^{n+} \quad + \quad H-R \quad \longrightarrow \quad [M]{-}N(H){-}R'^{(n-1)+} \quad + \quad \bullet R \qquad (3)$$
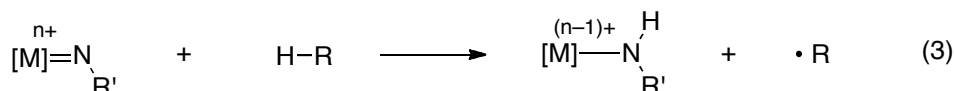
1-4. Author's previous work

• Synthesis and characterization of the first isolated iron imido complex $L^{Me}Fe(III)NAd$ (**1**) that performs intra- and intermolecular HAT reactions.[3]

Scheme 1. Intramolecular HAT by **1**

Scheme 2. Intermolecular HAT by **1**

1-5. This work

• Authors performed one of the first systematic studies on the kinetics and thermodynamics of HAT reactivity of an imido complex with any late TM using $L^{Me}Fe(III)NAd$ (**1**) by experimental and computational analysis.

2. Results and Discussion

2-1. HAT reaction of $1\cdot{}^t\textbf{BuPy}$

• While pyridine-free **1** is stable for several weeks at −45 °C, **1** showed HAT reactivity when ${}^t\textbf{BuPy}$ was added.

• $1\cdot{}^t\textbf{BuPy}$ is far less stable and decomposes to $3\cdot{}^t\textbf{BuPy}$ within a few hours at rt via intramolecular HAT (Scheme 1), and $1\cdot{}^t\textbf{BuPy}$ rapidly reacts with 1,4-cyclohexadiene (CHD) via intermolecular HAT (Scheme 2).

2-2. Thermodynamics of pyridine coordination to 1

• Equilibrium constants K_{eq} between **1** and $1\cdot{}^t\textbf{BuPy}$ were obtained by ^{1}H NMR titration in toluene-d_8 changing $[{}^t\textbf{BuPy}]_0$ (Table 1).

• van't Hoff plot gave $\Delta H_{eq} = -7.0(2)$ kcal mol^{-1}, $\Delta S_{eq} = -20.6(6)$ cal mol^{-1} K^{-1}, $\Delta G_{eq,\,298} = -0.9(3)$ kcal mol^{-1} that indicated very weak coordination.

• More electron-rich pyridine bound more strongly to **1**.

2-3. Kinetic studies of intramolecular HAT (Scheme 1)

• Conversion of **1** to $3\cdot{}^t\textbf{BuPy}$ was monitored by ^{1}H NMR in C$_6$D$_6$ at 40 °C to obtain pseudo-first-order rate constants k_{obs} at various concentrations of ${}^t\textbf{BuPy}$ (Figure 1).

• k_{obs} increased as $[{}^t\textbf{BuPy}]$ increased ($k_{obs} = 0$ when $[{}^t\textbf{BuPy}] = 0$)

➔ $1\cdot{}^t\textbf{BuPy}$ (not **1**) is the active species of HAT reaction.

• Saturation of k_{obs} from $[{}^t\textbf{BuPy}] \approx 0.2$ M indicated rapid pre-equilibrium of ${}^t\textbf{BuPy}$ association prior to the rate determining HAT.

• k_{intra} was calculated by fitting Eq 4 to the data in Figure 1 for 4 pyridines having different para substituents.

$$- \frac{d[1\cdot{}^t\textbf{BuPy}]}{dt} = k_{intra}\left(\frac{K_{eq}\,[1]_0\,[{}^t\textbf{BuPy}]_0}{1 + K_{eq}\,[{}^t\textbf{BuPy}]_0} \right) \quad (4)$$

• Hammet plot of k_{intra} against σ_p showed $\rho = -0.77(4)$ (Figure 2).

➔ More electron-rich pyridine led to faster HAT.

2-4. Kinetic studies of intermolecular HAT (Scheme 2)

• Addition of hydrocarbons with weak C−H bonds prevented intramolecular HAT and caused intermolecular HAT.

• The reaction of $1\cdot{}^t\textbf{BuPy}$ and CHD was monitored by ^{1}H NMR in toluene-d_8 at −51 °C (no intra-HAT) to obtain pseudo-first-order rate constants k_{obs} at various concentrations of CHD and ${}^t\textbf{BuPy}$ (Figures 3 and 4).

• Linear dependence of k_{obs} on [CHD] suggested rate determining HAT (Figure 3).

• Saturation of k_{obs} was also observed at lower concentration of $[{}^t\textbf{BuPy}]$ due to higher K_{eq} at −51 °C (Table 1, Figure 4).

• k_{inter} was calculated from the slope of Figure 3 based on $k_{obs} = 2\,k_{inter}[CHD]$ derived from Eq 5.

$$- \frac{d[1\cdot{}^t\textbf{BuPy}]}{dt} = 2\,k_{inter}\,[CHD]\,[1\cdot{}^t\textbf{BuPy}] \approx 2\,k_{inter}\,[CHD]\,[1]_0 = k_{obs}\,[1]_0 \quad (5)$$
$$\text{under saturation of } [{}^t\textbf{BuPy}]$$

• Large KIE value $k_H/k_D = 105 \pm 28$ for the reaction with CHD and CHD-d_8 supported rate determining HAT.

Table 1.

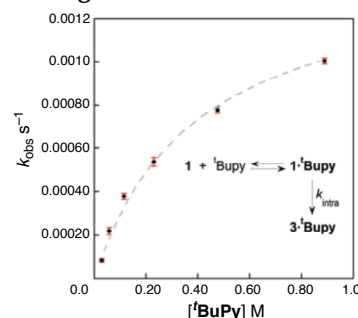| Pyridine	T (°C)	K_{eq} (M^{-1})
4-^{t}BuPy	−51	250 ± 20
4-^{t}BuPy	0	15.4 ± 0.5
4-^{t}BuPy	40	2.5 ± 0.1
4-Me$_2$NPy	40	4.7 ± 0.3
4-PhPy	40	1.8 ± 0.1
4-CF$_3$Py	40	0.8 ± 0.1

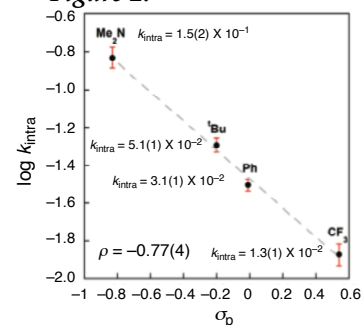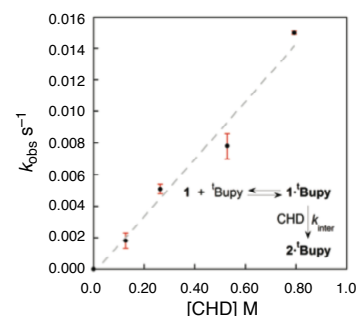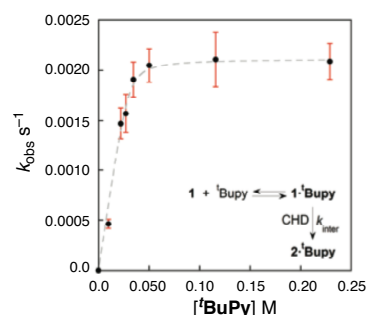*Figure 1.*

Figure 2.

Figure 3.

Figure 4.

2-5. Kinetic studies of intermolecular HAT with other substrates

• Rates of inter-HAT with **1·^{t}BuPy** did not correlate with homolytic BDE but were controlled by steric accessibility of a C–H bond to the imido nitrogen (entry 2 > 4 > 5, entry 2 > 3 > 6) partly due to steric hindrance from large imido N-substituent, β-diketiminate ligand, and added **^{t}BuPy.**

➔ Rare example of a system where there is no strong k_{HAT}/homolytic BDE relationship.

• Higher k_{inter} of indene than DHN can be explained by the difference of heterolytic BDE (entries 1 and 3)

Table 2. *Relationship between k_{inter} and BDEs*

Entry	Substrate		k_{inter} (M^{-1} s^{-1}) at –51 °C	k_{rel}	Homolytic BDE^a (kcal mol^{-1})	Heterolytic BDE^a (kcal mol^{-1})
1			$(1.9 \pm 0.2) \times 10^{-2}$	190	77	351
2		CHD	$(9.1 \pm 0.9) \times 10^{-3}$	90	71	375
3		DHN	$(1.56 \pm 0.04) \times 10^{-4}$	1.6	72	366
4		Me$_2$CHD	$(1.00 \pm 0.05) \times 10^{-4}$	1	71	376
5		Me$_4$CHD	0	0	71	375
6		DHA	0	0	74	359
7			0	0	89	–

^{a} Calculated at B3LYP/6-311++G(d,p)

➔ Proton-transfer character in TS of HAT, with positive charge on the metal fragment and negative charge on hydrocarbon (concerted but asynchronous proton transfer/electron transfer).

– Support (1): HAT in THF-d_8 containing electrolyte [^{n}Bu$_4$N][BAr$^F_4$] was 1.6 times faster than HAT in THF-d_8, which could be explained by the stabilization of charge built up in TS by polar environment.

– Support (2): More electron-rich pyridine led to faster HAT, which could be explained by increased Brønsted basicity of the imido nitrogen (2–3, Figure 2).

2-6. Computational studies

Table 3. *Intermolecular HAT with **1** and **1·^{t}BuPy***

	H/G kcal mol^{-1}	Fe=N$_{imido}$ Å	Spin density on N$_{imido}$		H/G kcal mol^{-1}	Fe=N$_{imido}$ Å	Spin density on N$_{imido}$
1 (Quartet)	0.0/0.0	1.70	0.26 e$^-$	**1·^{t}BuPy** (Quartet)	0.0/0.0	1.76	0.44 e$^-$
1 (Sextet)	11.7/11.9	1.75	1.07 e$^-$	**1·^{t}BuPy** (Sextet)	2.4/0.2	1.77	1.08 e$^-$
[**1** + CHD]‡ (Quartet)	5.5/22.2	1.83	–	[**1·^{t}BuPy** + CHD]‡ (Quartet)	9.7/24.8	1.88	–
[**1** + CHD]‡ (Sextet)	12.0/27.9	1.90	–	[**1·^{t}BuPy** + CHD]‡ (Sextet)	13.3/28.1	1.90	–

• ONIOM(B3LYP/6-311++G(d,p):UFF) calculation was performed (Table 3).

• **1** has quartet ground state (12 kcal mol^{-1} below sextet), which is consistent with EPR measurement and calculated bond distances and angles well agree with the crystal structure of **1** (e.g. Fe=N$_{imido, X-ray}$: 1.67 Å).

• **1·^{t}BuPy** has still quartet ground state but the addition of ^{t}**BuPy** decreased the quartet/sextet energy gap and increased Fe=N$_{imido}$ bond length (1.70 –> 1.76 Å).

• Although sextet of each complex **1** and **1·^{t}BuPy** has higher spin density on imido nitrogen than quartet, that did not lead to a significant enhancement of HAT reactivity.

• TSs have longer Fe=N$_{imido}$ bond (1.83–1.90 Å) than the complexes before TS (1.70–1.77 Å).

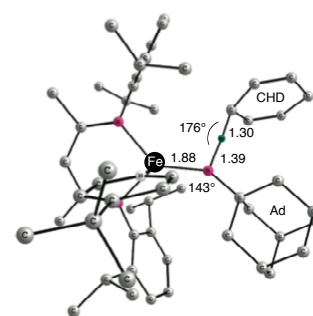• Linear geometry of N---H---C could explain the large KIE value caused by H tunneling (Figure 5).

• Calculation failed to predict relative reactivity of **1** and **1·^{t}BuPy** giving higher activation energy for **1·^{t}BuPy** (Authors don't mention it in the main text).

Figure 5. *TS geometry of* ***1·^{t}BuPy*** *+ CHD at quartet*

2-7. Why is **1•^tBuPy** much more reactive than **1**?

— Hypothesis (1): Coordination of **^tBuPy** weakens Fe=N π-bond ➔ ○

• Computation predicted longer Fe=N$_{imido}$ bond upon addition of **^tBuPy** (Table 3).

• Longer Fe–N bond in **1•^tBuPy** weakens π-donation of imido ligand into metal d-orbitals, resulting in higher basicity of imido nitrogen.

• Similar to the observation that increased basicity of the oxo ligand by the axial thiolate ligand led to faster HAT in iron–oxo complexes.[4]

— Hypothesis (2): Coordination of **^tBuPy** allows two-state reactivity ➔ ×

• Some synthetic Fe=O complexes with intermediate spin are known to react via TS with high spin state, which has lower barrier due to enhanced d–d exchange interactions: Accessible high-spin TS can facilitate HAT.[5]

• TS energy for sextet is calculated to be higher (not significantly lower) than quartet (Table 3).

— Hypothesis (3): **^tBuPy** binds to **2** more strongly than to **1** ➔ ○

Table 4. Activation Parameters Obtained by Eyring Plot

		$\Delta H^{\ddagger}$ kcal mol^{-1}	$\Delta S^{\ddagger}$ cal mol^{-1} K^{-1}	$\Delta G^{\ddagger}_{298}$ kcal mol^{-1}
1•^tBuPy	intra HAT	+14.6(5)	−18(2)	+20(1)
1	inter HAT	+12.2(3)	−33(2)	+22(1)
1•^tBuPy	inter HAT	+14.4(8)	−9(3)	+17(2)

Figure 6. Thermodynamic square by van't Hoff plot
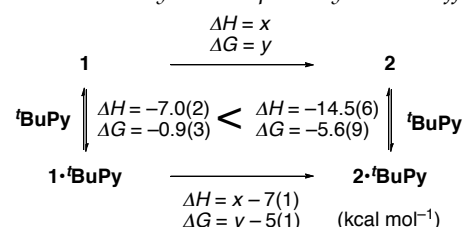
• Addition of **^tBuPy** resulted in $\Delta\Delta G^{\ddagger}_{298}$ = −5(2) kcal mol^{-1} (Table 4), which could be explained by thermodynamic driving force $\Delta\Delta G_{298}$ = −5(1) kcal mol^{-1} (Figure 6).

➔ More stabilization of the product **2** by **^tBuPy** is thermodynamic driving force for HAT.

3. Conclusion
• The first thorough study of the mechanism of HAT reactivity of an imidoiron complex.
• HAT is a rate determining step.
• HAT with proton-transfer character was proposed with proton-transfer slightly preceding electron transfer.
• Addition of **^tBuPy** dramatically enhanced the HAT reactivity towards C–H bonds due to the increased basicity of the imido nitrogen and increased thermodynamic driving force to form the product **2•^tBuPy**.
• HAT reactivity was not controlled by homolytic BDE of C–H bonds but steric hindrance of a substrate and acidity of C–H bonds.
• Improvement of HAT reactivity by ligand design is in progress.

4. References

[1] Huynh, M. H. V.; Meyer, T. J. *Chem. Rev.* **2007**, *107*, 5004–5064.

[2] Bell, R. P. *Proc. R. Soc. London, Ser. A* **1936**, 154, 414–429.

[3] a) Eckert, N. A.; Vaddadi, S.; Stoian, S.; Lachicotte, R. J.; Cundari, T. R.; Holland, P. L. *Angew. Chem., Int. Ed.* **2006**, *45*, 6868–6871. b) Cowlye, R. E.; DeYonker, N. J.; Eckert, N. A.; Cundari, T. R.; DeBeer, S.; Bill, E.; Ottenwaelder, X.; Flaschenriem, C. J.; Holland, P. L. *Inorg. Chem.* **2010**, *49*, 6172–6187.

[4] a) Green, M. T.; Dawson, J. H.; Gray, H. B. *Science* **2004**, *304*, 1653–1656. b) Behan, R. K.; Hoffart, L. M.; Stone, K. L.; Krebs, C.; Green, M. T. *J. Am. Chem. Soc.* **2006**, *128*, 11471–11474.

[5] Shaik, S.; Hirao, H.; Kumar, D. *Acc. Chem. Res.* **2007**, *40*, 532–542.